ACS APPLIED POLYMER MATERIALS

pubs.acs.org/acsapm Letter

Electrophilic Effect of Polysulfide Cations Induces the Formation of Li^+-Transport-Enhanced Polymer Electrolyte

Hongxu Zhou, Xiaoning Wang, Yiyang Zhao, Jingang Zheng, Hao Huang, Weichen Han, Hongwei Zhao, Han Zhang, Lixiang Li, Baigang An, and Chengguo Sun*

Cite This: *ACS Appl. Polym. Mater.* 2025, 7, 12145−12150 Read Online

ACCESS | Metrics & More | Article Recommendations | Supporting Information

ABSTRACT: Slow ion transport kinetics hinder the development of solid polymer electrolytes in lithium metal batteries. Herein, we adopt the electron-deficient $Li_3S_6^+$ as an electrophilic initiator to induce the ring-opening copolymerization of 1,3-dioxolane and ethylene glycol diglycidyl ether in a precursor solution. The $Li_3S_6^+$ in prepared polymer electrolyte (FITSE) improves both ionic conductivity and Li^+ transference number while generating a gradient sulfur-containing SEI layer to promote uniform lithium deposition. The Li||FITSE||LFP cell delivers a high initial capacity of 138.8 mAh g^{-1} with a capacity retention of 94.6% over 250 cycles at 1 C and maintains a capacity of 60.96 mAh g^{-1} over 130 cycles even at −10 °C.

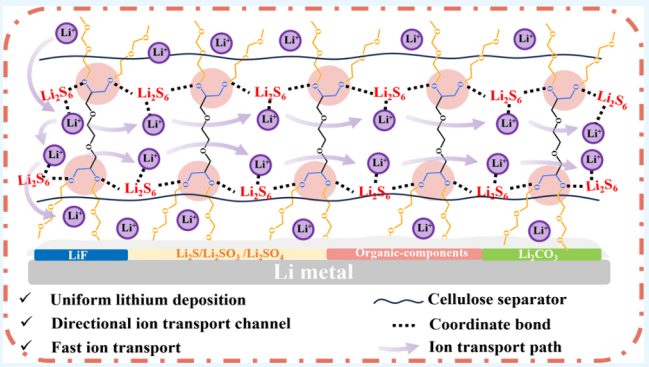

KEYWORDS: *ion transport kinetics, electrophilic effect, polysulfide cations, polymer network, lithium deposition*

1. INTRODUCTION

Lithium metal batteries (LMBs) dominate portable electronic devices due to the use of lithium metal anodes, which offer a unique high theoretical specific capacity (3860 mAh g^{-1}) and extremely low reduction potential (−3.04 V vs standard hydrogen electrode).[1] However, LMBs with liquid electrolytes still face a potential leakage risk and poor chemical stability toward high-voltage cathode materials. All-solid-state electrolytes are suggested to make up for the above-mentioned shortcomings.[2] Among various kinds of solid-state electrolytes, solid polymer electrolytes (SPEs) have received tremendous attention in terms of their flexibility and excellent electrode interface compatibility.[3] Over the years, SPEs have evolved from traditional polyether-based SPEs (such as PEO, 10^{-7}−10^{-5} S cm^{-1}) with limited ionic conductivity[4] to complex architectures incorporating cross-linked polymer networks,[5] block copolymer electrolytes,[6] and organic−inorganic composite electrolytes.[7] Unfortunately, the lack of fluidity in polymer-based electrolytes impedes the efficient ion migration in solid-state phases.[8]

The strategy of in situ polymerizing liquid monomers enables the precursor solution to infiltrate the electrodes and electrolyte, facilitating the formation of ion transport networks.[9,10] In contrast to the copolymerization of alkenes, the linear polydioxolane (PDOL) derived from the ring-opening polymerization of 1,3-dioxolane (DOL) features superior interfacial compatibility with a lithium metal anode and ionic conductivity (>0.1 mS cm^{-1}, 25 °C).[11] The ring-opening polymerization of DOL can be initiated through several strategies, including electrochemical activation,[12] electrophilic initiators,[13] and free radical induction.[14] Recently, Lewis acids ($LiPF_6$, $Al(OTf)_3$, $InCl_3$, etc.) have emerged as effective and selective ring-opening strategies. They activate the monomer through coordination with the oxygen atom as electrophilic initiators, enabling the reaction to proceed under milder conditions.[15] However, the above approaches of ring-opening DOL resulted in substantial residual DOL in overly rapid polymerization, thereby deteriorating the solid electrolyte interface (SEI) on the lithium anode.[16] Moreover, the linear PDOL is apt to fail in suppressing lithium dendrite growth due to its insufficient mechanical strength. Therefore, developing an ideal polymerization initiator that can effectively induce ring-opening polymerization and simultaneously promote the stable SEI layer remains a current research focus.

We utilized the cationic compound ($Li_3S_6^+$) derived from lithium polysulfides to activate epoxy groups, promoting the open-chain addition reaction between polymer monomers. Previously, the application of polysulfides in LIBs was limited due to the instability in air.[17] Herein, a polysulfide-loaded cellulose separator (denoted as Li_2S_6@CS) was employed as

Received: July 9, 2025
Revised: September 16, 2025
Accepted: September 16, 2025
Published: September 18, 2025

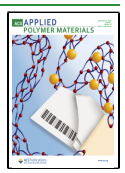

https://doi.org/10.1021/acsapm.5c02505
ACS Appl. Polym. Mater. 2025, 7, 12145−12150

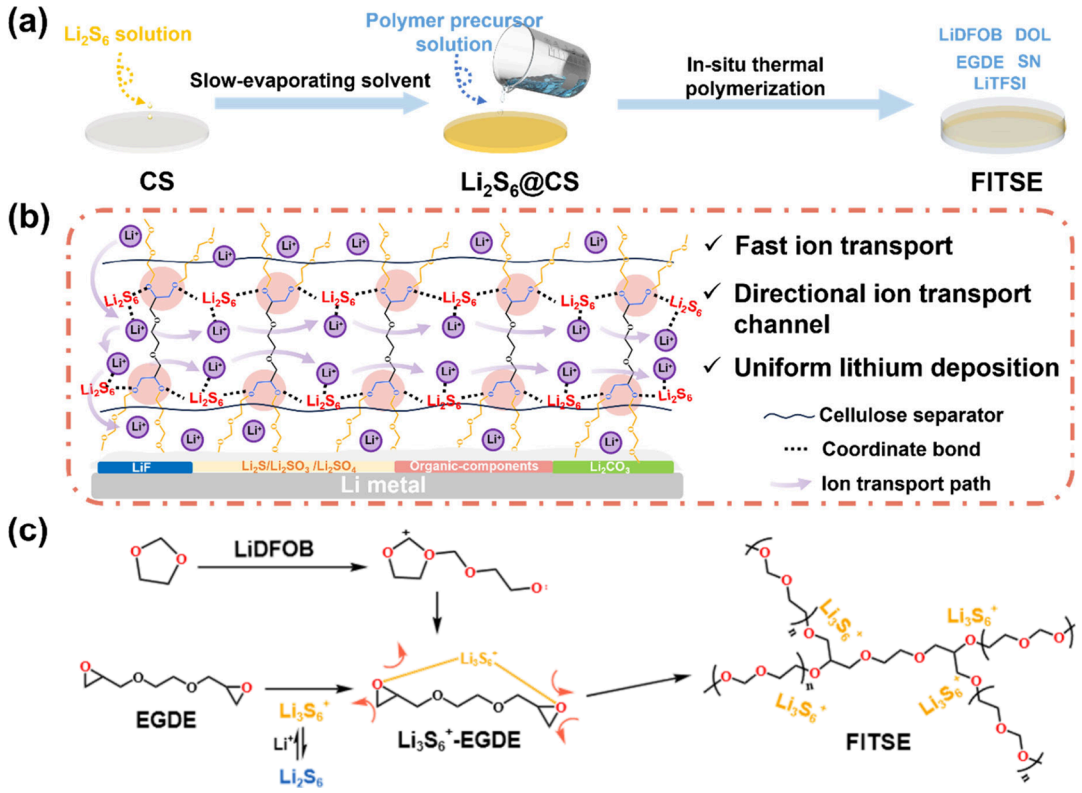

Figure 1. (a) Schematic diagram of FITSE prepared by modifying the separator and in situ polymerization, with an enlarged illustration on the right showing ion transport within FITSE. (b) Polymerization mechanism diagram of FITSE. (c) The polymerization mechanism diagram of FITSE.

the supporting scaffold and subsequently impregnated with the polymer precursor solution consisting of lithium salts, succinonitrile (SN), ethylene glycol diglycidyl ether (EGDE) monomers, and DOL. Polysulfides first spontaneously react with lithium salts in the precursor solution to generate polysulfide cations ($Li_3S_6^+$), which then act as electrophiles to attack the epoxy groups of EGDE and form active intermediates ($Li_3S_6^+$-EGDE). Difluoro(oxalato)borate(1−) (LiDFOB)-derived DOL radicals easily attack the $Li_3S_6^+$-EGDE intermediates and initiate a ring-opening polymerization reaction. Finally, the ring-opened EGDE copolymerizes with DOL to form extended polymer long chain. $Li_3S_6^+$ not only accelerates the copolymerization of DOL and EGDE but also acts as fast ion conductors uniformly distributed around the polymerization sites after EGDE ring-opening to further construct an efficient ion transport network (FITSE). More importantly, polysulfides can also generate high-valence sulfur-containing species during cycling, which are beneficial for SEI formation and uniform lithium deposition. In contrast to linear PDOL, FITSE exhibits superior stretchability and dendrite suppression. It achieves excellent ionic conductivity (5.91×10^{-4} S cm^{-1}, 25 °C) and an electrochemical stability window (~5.1 V). The Li||Li cells with FITSE exhibited stable plating/stripping of lithium metal at a current density of 0.5 mA cm^{-2}, while Li||FITSE||LFP cells maintained high specific capacity even at low temperature (−10 °C) and high current density (3 C).

2. RESULTS AND DISCUSSION

The preparation process and design concept of FITSE are illustrated in Figure 1. Li_2S_6 was selected as the key polysulfide in this paper due to its high ionic conductivity.[18] First, the lithium polysulfide (Li_2S_6) solution was dropped onto a cellulose separator (CS) to obtain the Li_2S_6-loaded separator (designated as Li_2S_6@CS), followed by injecting the polymer precursor solution containing lithium salts, succinonitrile (SN), ethylene glycol diglycidyl ether (EGDE) monomers, and DOL into Li_2S_6@CS (Figure 1a) and curing at 60 °C for 12 h to obtain the electrolyte membrane (FITSE). The polymer matrix can not only provide the adsorption sites for the lithium-ion coordination but also provide combination sites for the polysulfide ions. The incorporation of polysulfides further regulates Li^+ migration in the electrolyte membrane (Figure 1b). The polymerization mechanism in FITSE is shown in Figure 1c. Li_2S_6 readily binds with Li^+ from LiTFSI to form cationic polysulfides ($Li_3S_6^+$).[19] Owing to the Lewis acid property, $Li_3S_6^+$ is prone to function as the electrophilic initiator, attacking electron-deficient regions of the reactants. Therefore, $Li_3S_6^+$ can react with the electron-rich epoxy groups of EGDE to generate the complexed active intermediates ($Li_3S_6^+$-EGDE) in a process termed the electrophilic reaction pathway.[11,20] Subsequently, DOL radicals induced by LiDFOB attack the $Li_3S_6^+$-EGDE complex, triggering ring-opening copolymerization with DOL and facilitating extension of the polymer network. However, the detached $Li_3S_6^+$ were uniformly dispersed around the EGDE chain segments of the copolymer via electrostatic adsorption, forming ion transport channels to promote Li^+ migration in FITSE.

Electron spray ionization mass spectrometry (ESI-MS) was employed to detect $Li_3S_6^+$ and analyze sulfur species in different Li_2S_6 solution. With extra LiTFSI, the intensity of the cationic $Li_3S_6^+$ (m/z = 303, with one DME as the solvation

https://doi.org/10.1021/acsapm.5c02505
ACS Appl. Polym. Mater. 2025, 7, 12145−12150

sheath) characteristic peak increases significantly (Figure S1), demonstrating the strong association tendency between Li_2S_6 and Li^+. LiDFOB-derived DOL radicals then easily attack the $Li_3S_6^+$-EGDE intermediates and initiate a ring-opening polymerization reaction. During the polymerization reaction process, LiDFOB plays the key role to induce the elongation of the DOL chain, while the other solution remained in the flow state after keeping them at 50 °C for 5 days (Figure S2).

The optical photos of the Li_2S_6 separator and polymer matrix after polymerization are illustrated in Figure 2a, where

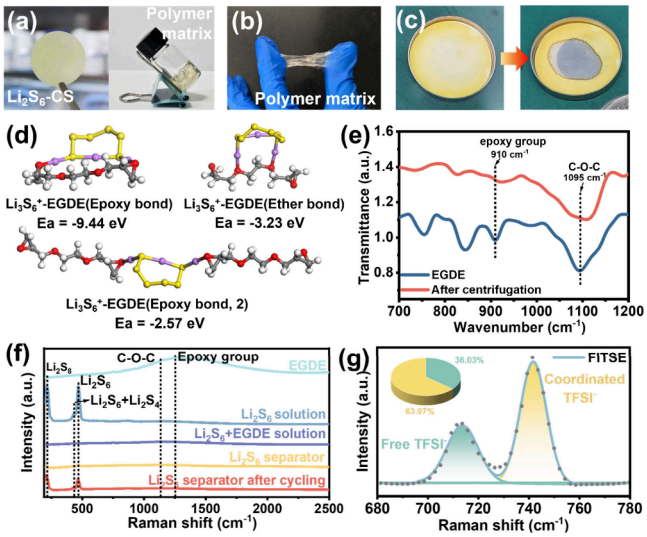

Figure 2. (a) Optical photos of Li_2S_6-CS and the polymerized polymer matrix. (b) Stretch properties of the polymer matrix. (c) Optical photos of the Li_2S_6 separator and polymer matrix after polymerization. (d) Interaction energy of the cation polysulfide ($Li_3S_6^+$) binding with different functional groups in the EGDE monomer. (e) FTIR spectra of EGDE and precipitates produced by mixing EGDE in a Li_2S_6 solution. (f) Raman results of different reaction stages between polysulfides and EGDE. (g) Peak fitting analysis of Raman spectra for FITSE in relation to the Li_2S_6 separator.

the Li_2S_6 separator appears light yellow, and the polymer matrix exhibits a homogeneous and transparent appearance (Figure S3 shows the optical image of the polymer precursor solution). Furthermore, the polymer matrix shows excellent stretchability (Figure 2b). After compositing with Li_2S_6@CS, the FITSE demonstrates both plasticity and gel-like characteristics and also maintains superior stretchability inherited from the polymer matrix compared to the TF separator (Figure S4). During the experiment, it was surprisingly observed that Li_2S_6@CS rapidly faded after dropping the polymer precursor solution (Figure 2c), indicating reactions with solution components. Subsequently, the formation of $Li_3S_6^+$-EGDE active intermediates was visualized (Figure S5). In contrast, the LiTFSI-containing Li_2S_6 solution produced heavy precipitation after adding EGDE, further indicating the electrophilic reaction of $Li_3S_6^+$. Li_2S_6 was introduced into the mixed solution containing two lithium salts and SN to monitor the precursor changes. The solution presented the characteristic color of polysulfides, which faded rapidly after adding EGDE, followed by the formation of a turbid precipitate after placing (Figure S6). This observation is consistent with the results shown in Figure S5. Subsequently, as the degree of polymerization increased, the polymer matrix gradually regained a brown-yellow appearance and became transparent. The color transformation in the process indicates that polysulfides are re-released after EGDE ring-opening triggered by LiDFOB, which further proves the complexation between polysulfides and epoxy groups in EGDE.

The binding energy of three addition products revealed that the complex formed between one $Li_3S_6^+$ and two epoxy groups of one EGDE showed the lowest binding energy (−9.44 eV), indicating a relatively stable state from a thermodynamic perspective (Figure 2d). Furthermore, the Fourier transform infrared (FTIR) analysis of the precipitated addition product from the polymer precursor after adding Li_2S_6 showed a shift in the epoxy bond characteristic peak of EGDE from 910 cm^{-1} to 924 cm^{-1}, demonstrating the interaction between the polysulfides and epoxy groups (Figure 2e). The characteristic peaks of Raman at 211, 432, and 465 cm^{-1} in the Li_2S_6 solution correspond to a Li_2S_8, Li_2S_6, and Li_2S_4 mixture and Li_2S_6 (Figure 2f).[21,22] This is attributed to the disproportionation reaction of Li_2S_6.[23] All polysulfide-related peaks disappeared after adding EGDE, along with C−O−C and epoxy group signals from EGDE. After cycling in the LFP||FITSE||Li cell, polysulfides reappeared in the electrolyte,

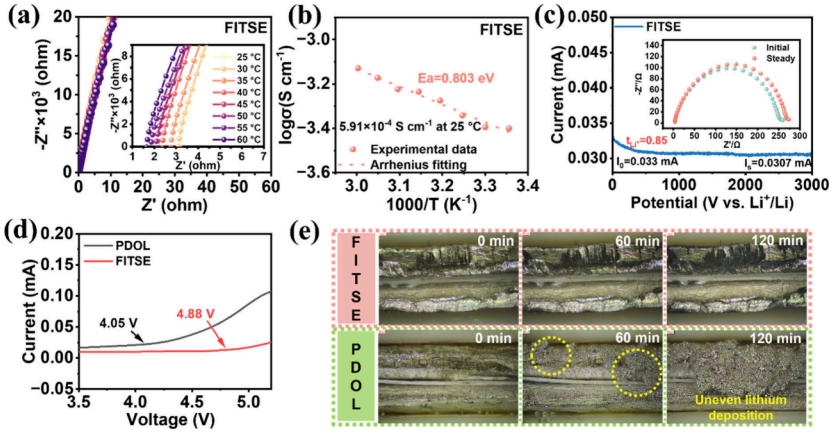

Figure 3. (a) Nyquist plots and (b) Arrhenius curve of FITSE at different temperatures. (c) Chronoamperometry profile of Li||FITSE||Li symmetric batteries and the Nyquist impedance spectra before and after polarization. (d) LSV curves of PDOL and FITSE. (d) In situ optical microscopy observation of lithium deposition using different electrolytes with increasing discharging time. (e) In situ optical microscopy observation of lithium deposition using different electrolytes with increasing discharging time.

https://doi.org/10.1021/acsapm.5c02505
ACS Appl. Polym. Mater. 2025, 7, 12145−12150

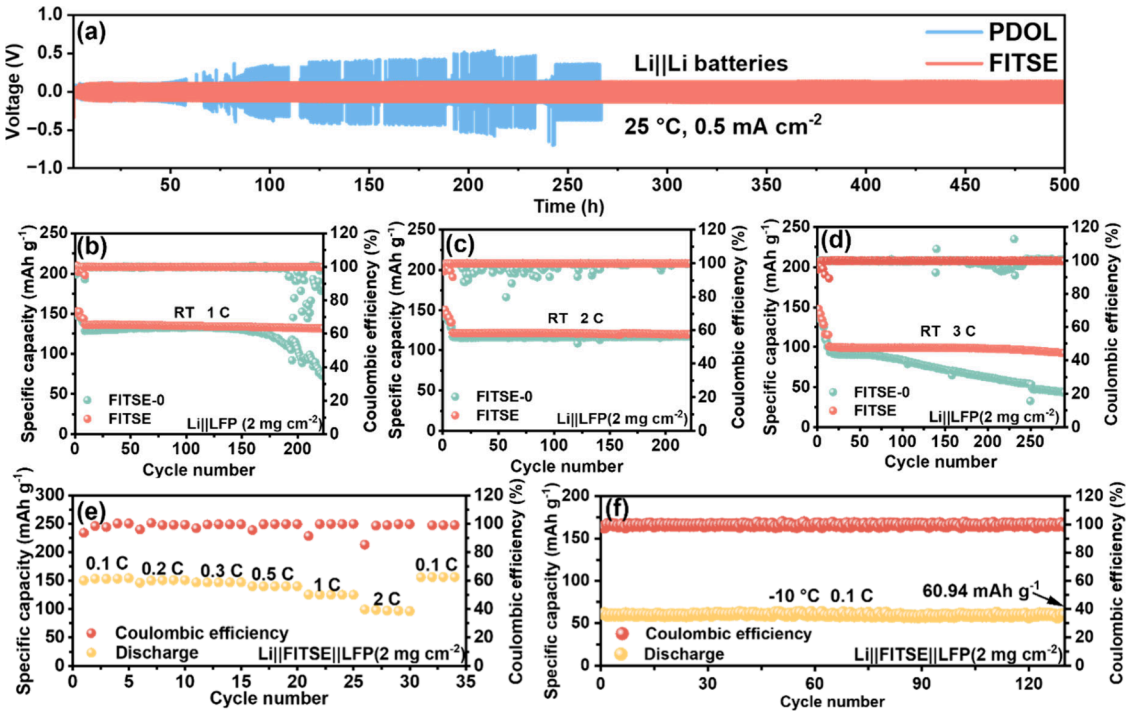

Figure 4. (a) Cycling performance of Li||Li symmetric batteries with FITSE and FITSE-0. Cycling stability of Li||FITSE-0||LFP and Li||FITSE||LFP at (b) 1 C, (c) 2 C, and (d) 3 C. (e) Rate performance of the Li||FITSE||LFP cell at step-increased C-rates. (f) Cycling stability of the cell with FITSE under a rate of 0.1 C at −10 °C.

indicating their release and immobilization within the electrolyte structure during cycling. Moreover, the free $TFSI^-$ and coordinated $TFSI^-$ were further detected by Raman analysis. Compared with Li_2S_6-free SPEs (Figure S7), the higher proportion of free $TFSI^-$ in FITSE (Figure 2g) proves enhanced lithium salt dissociation and improved Li^+ transport efficiency. The nuclear magnetic resonance (NMR) spectra of ^7Li confirmed the coordination environment in SPEs (Figure S8). The ^7Li NMR spectrum showed a downfield shift in polymerized EGDE+Li_2S_6 compared to the pure Li_2S_6 solution, indicating reduced electron density around Li^+ and an increase in free Li^+,[24] further verifying the Raman results from the Li_2S_6-containing separator.

To investigate the effect of Li_2S_6 on the ion transport kinetics of the FITSE electrolyte, the ionic conductivity and the corresponding activation energy of FITSE with varying Li_2S_6 content were measured (Figure 3a,b, Figure S9a,b, Figure S10a,b, and Figure S11a,b). Different amounts of Li_2S_6 were named FITSE-x (x = 0, 10, 20, 30 μL). As a result, FITSE-10 showed the highest ionic conductivity (5.91×10^{-4} S cm^{-1}, 25 °C) and the lowest activation energy (0.803 eV) and was consequently selected for subsequent electrochemical tests (abbreviated as FITSE). In addition, FITSE achieved a high Li^+ transference number (t_{Li+} = 0.85), which is 1.33 times higher than that of FITSE-0 (Figure 3c, Figures S9c–S11c). The results indicate polysulfide can improve the ionic conductivity and lower the ionic transfer energy barrier for enhanced ionic transport kinetics in the electrolyte. The electrochemical stability window of FITSE is over 4.8 V (Figure 3d), endowing superior antioxidant capabilities compared to linear PDOL (4.05 V).[11,25] The curves of cyclic voltammetry (CV) have a highly consistent redox behavior, indicating the superior electrochemical stability of FITSE (Figure S12). To visualize the lithium deposition behavior during cycling, in situ optical microscopy images reveal uniform lithium deposition with negligible dendrite growth during discharge in FITSE, in contrast to uneven lithium deposition in the PDOL electrolyte (Figure 3e). This result demonstrates that FITSE contributes to Li plating/stripping processes.

Rate performances of the Li||Li symmetric cell with FITSE reveal superior lithium deposition/stripping behavior, maintaining a stable square-wave voltage−time curve even at 1.2 mA cm^{-2}. However, the Li||PDOL||Li symmetric cell exhibits a large overpotential, and a sawtooth pattern followed by short-circuiting occurs (Figure S13). The Li||Li symmetric cell with FITSE has maintained a stable low overvoltage of 15 mV over 500 h at a current density of 0.5 mA cm^{-2}, demonstrating its excellent lithium deposition/stripping behavior (Figure 4a). Unfortunately, after only 50 cycles, the overpotential fluctuation of the cell with PDOL increased steeply, indicating that the electrode−electrolyte interface was severely degraded. In addition, we also evaluated the stability of symmetric cells assembled with FITSE-x (x = 0, 20, 30). Their overpotentials were slightly higher than that of FITSE (Figure S14). We speculate that excessive polysulfides can affect the interface layer of the lithium anode. Subsequently, the lithium metal was further analyzed by SEM and in-depth X-ray photoelectron spectroscopy (XPS) spectra to investigate the formation of the SEI layer (Figures S15, S16). As the etching time increases, the gradient architecture with an organic-rich outer layer and inorganic-rich inner layer significantly can enhance the stability and cycling performance of batteries.[26,27] The Li||LFP cell was assembled to evaluate the performance of the FITSE electrolyte under practical charge−discharge conditions. The Li||LFP cell using FITSE exhibits 153.4, 150.8, 147, 140.2, 125.4, and 98.4 mAh g^{-1} at a rate of 0.1, 0.2, 0.3, 0.5, 1, and 2 C, respectively (Figure 4e). Figure 4b–d show the cycling

https://doi.org/10.1021/acsapm.5c02505
ACS Appl. Polym. Mater. 2025, 7, 12145−12150

performance of Li||LFP cells with FITSE and FITSE-0 at 1, 2, and 3 C, respectively. The cell with FITSE delivers a higher initial discharge capacity of 138.8 mAh g^{-1} and exhibits a high-capacity retention of over 94.6% with an average CE of 99.87% after 250 cycles at 1 C. Even at higher current density, the Li||FITSE||LFP cell also exhibits excellent cycling stability (Figure 4d). In contrast, the cell with FITSE-0 exhibits a lower initial capacity of 128.3 mAh g^{-1} at 1 C, and its capacity decreases as the current density increases, which were all lower than those of the Li||FITSE||LFP cells. Furthermore, the electrochemical performance of Li||PDOL||LFP cells from the recently published literature was compared to further demonstrate the advantages of FITSE (Table S1). Even at −10 °C, the Li||LFP cell with FITSE can also deliver at least stable cycling of 130 cycles at 0.1 C.

3. CONCLUSION

In summary, a high-performance solid polymer electrolyte (FITSE) with fast ion transport and uniform lithium deposition capability was designed through a $Li_3S_6^+$ electrophilic modulation strategy. $Li_3S_6^+$ initiates the copolymerization of EGDE and DOL through reactive intermediates ($Li_3S_6^+$-EGDE). The detached $Li_3S_6^+$ uniformly distributes around the polymerization sites, forming ion-conducting pathways and regulating the ion transport kinetics in FITSE, achieving ionic conductivity of up to 5.91×10^{-4} S cm^{-1} (25 °C). FITSE shows a high t_{Li+} (0.88) and electrochemical stability window (~5.1 V) to imply excellent ion transport kinetics. Furthermore, polysulfide-derived high-valence sulfur-containing products (Li_2SO_3 and Li_2SO_4) promote uniform lithium deposition during cycling, allowing the Li||FITSE||Li cell to stably cycle for 500 h at 0.5 mA cm^{-2}. The Li||FITSE||LFP cells also deliver outstanding rate performance and cycling stability and operate stably even at −10 °C.

■ ASSOCIATED CONTENT

Supporting Information

The Supporting Information is available free of charge at https://pubs.acs.org/doi/10.1021/acsapm.5c02505.

Experimental section and analytical characterization, graphs, and tables (PDF)

■ AUTHOR INFORMATION

Corresponding Author

Chengguo Sun − *School of Chemical Engineering, University of Science and Technology Liaoning, Anshan 114051, China; School of Chemical Engineering, Nanjing University of Science and Technology, Nanjing 210094, China;* orcid.org/0000-0003-3580-2153; Email: sunyangguo2004@163.com

Authors

Hongxu Zhou − *School of Chemical Engineering, University of Science and Technology Liaoning, Anshan 114051, China*

Xiaoning Wang − *School of Chemical Engineering, University of Science and Technology Liaoning, Anshan 114051, China*

Yiyang Zhao − *School of Chemical Engineering, University of Science and Technology Liaoning, Anshan 114051, China*

Jingang Zheng − *School of Chemical Engineering, University of Science and Technology Liaoning, Anshan 114051, China*

Hao Huang − *School of Chemical Engineering, University of Science and Technology Liaoning, Anshan 114051, China*

Weichen Han − *School of Chemical Engineering, University of Science and Technology Liaoning, Anshan 114051, China*

Hongwei Zhao − *School of Chemical Engineering, University of Science and Technology Liaoning, Anshan 114051, China*

Han Zhang − *School of Chemical Engineering, University of Science and Technology Liaoning, Anshan 114051, China;* orcid.org/0000-0001-6905-0952

Lixiang Li − *School of Chemical Engineering, University of Science and Technology Liaoning, Anshan 114051, China*

Baigang An − *School of Chemical Engineering, University of Science and Technology Liaoning, Anshan 114051, China;* orcid.org/0000-0001-6111-8166

Complete contact information is available at: https://pubs.acs.org/10.1021/acsapm.5c02505

Author Contributions

Hongxu Zhou: Writing—review and editing, Writing—original draft, Data curation, Conceptualization. **Xiaoning Wang:** Investigation, Formal analysis. **Yiyang Zhao:** Writing—review and editing, Data curation. **Jingang Zheng:** Writing—review and editing, Software. **Hao Huang:** Writing—review and editing, Visualization. **Weichen Han:** Data curation, Investigation. **Hongwei Zhao:** Writing—review and editing. **Han Zhang:** Investigation. **Lixiang Li:** Writing—review and editing, Investigation. **Baigang An:** Writing—review and editing, Validation, Supervision. **Chengguo Sun:** Writing—review and editing, Validation, Supervision, Investigation, Funding acquisition, Conceptualization.

Notes

The authors declare no competing financial interest.

■ ACKNOWLEDGMENTS

The authors gratefully acknowledge financial support by the National Natural Science Foundation of China (11972178, 52371224, and 22578219), the Nature Science Foundation of Liaoning Province (2023-BS-184), Distinguished Professor Project of Education Department of Liaoning, and the Open Project Found of Key Laboratory of Energy Materials and Electrochemistry Liaoning Province.

■ REFERENCES

(1) Li, J.; Jing, M.-X.; Li, R.; Li, L.-X.; Huang, Z.-H.; Yang, H.; Liu, M.-Q.; Hussain, S.; Xiang, J.; Shen, X.-Q. Al_2O_3 fiber-reinforced polymer solid electrolyte films with excellent lithium-ion transport properties for high-voltage solid-state lithium batteries. *ACS Appl. Polym. Mater.* **2022**, *4* (10), 7144−7151.

(2) Wu, M.; Bhargav, A.; Cui, Y.; Siegel, A.; Agarwal, M.; Ma, Y.; Fu, Y. Highly reversible diphenyl trisulfide catholyte for rechargeable lithium batteries. *ACS Energy Lett.* **2016**, *1* (6), 1221−1226.

(3) Wang, J.; Zhang, Y.; Ye, W.; Guo, K.; Zhou, X.; Xue, Z. Facile fabrication of polymer electrolytes with branched structure via deep eutectic electrolyte-enabled in situ polymerizations. *ACS Macro Lett.* **2024**, *13* (2), 166−173.

(4) Pei, F.; Wu, L.; Lin, W.; Zhang, Y.; Kang, Q.; Zhang, F.; Shen, Y.; Gao, Q.; Huang, Z.; Huang, Y. Progress and perspectives on molecular design of crosslinked polymer electrolytes for solid-state lithium batteries. *Annu. Rev. Mater. Res.* **2025**, *1*, No. 100013.

(5) Wu, L.; Pei, F.; Cheng, D.; Zhang, Y.; Cheng, H.; Huang, K.; Yuan, L.; Li, Z.; Xu, H.; Huang, Y. Flame-retardant polyurethane-based solid-state polymer electrolytes enabled by covalent bonding for lithium metal batteries. *Adv. Funct. Mater.* **2024**, *34* (16), No. 2310084.

(6) Lee, H.; Kim, J.; Park, M. J. Block copolymer electrolytes with double primitive cubic structures: enhancing solid-state lithium

conduction via lithium salt localization. *ACS Nano* **2025**, *19* (1), 1251−1259.
(7) Chen, A.; Li, N.; Sun, C.; Qin, Y.; Qi, L.; Zhang, H.; Bao, H. A novel flexible composite solid electrolyte based on 3D network structural inorganic Si-Zr-OC fiber film. *Chem. Eng. J.* **2025**, *520*, No. 166104.
(8) Tong, R. A.; Huang, Y.; Feng, C.; Dong, Y.; Wang, C. A. In-situ polymerization confined PEGDME-based composite quasi-solid-state electrolytes for lithium metal batteries. *Adv. Funct. Mater.* **2024**, *34* (30), No. 2315777.
(9) Wei, Z.; Chen, S.; Wang, J.; Wang, Z.; Zhang, Z.; Yao, X.; Deng, Y.; Xu, X. Superior lithium ion conduction of polymer electrolyte with comb-like structure via solvent-free copolymerization for bipolar all-solid-state lithium battery. *J. Mater. Chem. A* **2018**, *6* (27), 13438−13447.
(10) Zhou, H.; Xie, J.; Bao, L.; Qiao, S.; Sui, J.; Wang, J. Poly(carbonate)-based ionic plastic crystal fast ion-conductor for solid-state rechargeable lithium batteries. *J. Energy Chem.* **2022**, *73*, 360−369.
(11) Yang, S. J.; Yuan, H.; Yao, N.; Hu, J. K.; Wang, X. L.; Wen, R.; Liu, J.; Huang, J. Q. Intrinsically safe lithium metal batteries enabled by thermo-electrochemical compatible in situ polymerized solid-state electrolytes. *Adv. Mater.* **2024**, *36* (35), No. e2405086.
(12) Kong, L.; Zhan, H.; Li, Y.; Zhou, Y. In situ fabrication of lithium polymer battery basing on a novel electro-polymerization technique. *Electrochem. Commun.* **2007**, *9* (10), 2557−2563.
(13) Liu, Q.; Wang, L.; He, X. Toward practical solid-state polymer lithium batteries by in situ polymerization process: a review. *Adv. Energy Mater.* **2023**, *13* (30), No. 2300798.
(14) Shen, T.; Yu, Q.; Wei, J.; Wang, Y.; Wang, H.; Li, Z.; Ma, X.; Sun, J.; Ma, J.; Tie, Z.; Jin, Z. Electrolyte anion-initiated in situ polymerization of dioxolane-derived gel electrolytes for dendrite-resistant and separator-free lithium metal batteries. *Nano Lett.* **2025**, *25* (25), 10102−10113.
(15) Liu, Z.; Xi, M.; Sheng, R.; Huang, Y.; Ding, J.; Tan, Z.; Li, J.; Zhang, W.; Wang, Y. $Zn(TFSI)_2$-mediated ring-opening polymerization for electrolyte engineering toward stable aqueous zinc metal batteries. *Nano-Micro Lett.* **2025**, *17* (1), 120.
(16) Sun, Z.; Yang, J.; Wu, Y.; Meng, F.; Niu, Y.; Xu, H.; Zhu, Y.; Hong, B.; Chen, Z.; Zhu, J.; He, Q.; Wu, G.; Chen, W. Stabilizing residual monomers within in situ polymerized electrolytes for high-voltage lithium metal batteries. *J. Am. Chem. Soc.* **2025**, *147*, 18064−18073.
(17) Fang, R.; Xu, B.; Grundish, N. S.; Xia, Y.; Li, Y.; Lu, C.; Liu, Y.; Wu, N.; Goodenough, J. B. Li_2S_6-integrated PEO-based polymer electrolytes for all-solid-state lithium-metal batteries. *Angew. Chem., Int. Ed.* **2021**, *133* (32), 17842−17847.
(18) Yao, W.; Liao, K.; Lai, T.; Sul, H.; Manthiram, A. Rechargeable metal-sulfur batteries: key materials to mechanisms. *Chem. Rev.* **2024**, *124* (8), 4935−5118.
(19) Song, Y.-W.; Shen, L.; Yao, N.; Li, X.-Y.; Bi, C.-X.; Li, Z.; Zhou, M.-Y.; Zhang, X.-Q.; Chen, X.; Li, B.-Q.; Huang, J.-Q.; Zhang, Q. Cationic lithium polysulfides in lithium−sulfur batteries. *Chem.* **2022**, *8* (11), 3031−3050.
(20) Fang, Z.; Luo, Y.; Liu, H.; Hong, Z.; Wu, H.; Zhao, F.; Liu, P.; Li, Q.; Fan, S.; Duan, W.; Wang, J. Boosting the oxidative potential of polyethylene glycol-based polymer electrolyte to 4.36 V by spatially restricting hydroxyl groups for high-voltage flexible lithium-ion battery applications. *Adv. Sci.* **2021**, *8* (16), No. e2100736.
(21) Zhao, Z.; Pan, Y.; Chen, H.; Wang, X.; Huang, Y.; Yi, S.; Niu, B.; Long, D.; Zhang, Y. A lithium-affinitive covalent organic polymer network functionalized separator for dendrite-free and high-durability lithium−sulfur batteries under harsh conditions. *Adv. Funct. Mater.* **2024**, *34* (37), No. 2402182.
(22) Kang, X.; He, T.; Niu, S.; Zhang, J.; Zou, R.; Zhu, F.; Ran, F. Precise design of a 0.8 nm pore size in a separator interfacial layer inspired by a sieving effect toward inhibiting polysulfide shuttling and promoting Li(+) diffusion. *Nano Lett.* **2024**, *24* (33), 10007−10015.
(23) Liu, R.; Wei, Z.; Peng, L.; Zhang, L.; Zohar, A.; Schoeppner, R.; Wang, P.; Wan, C.; Zhu, D.; Liu, H.; Wang, Z.; Tolbert, S. H.; Dunn, B.; Huang, Y.; Sautet, P.; Duan, X. Establishing reaction networks in the 16-electron sulfur reduction reaction. *Nature* **2024**, *626* (7997), 98−104.
(24) Wu, L.; Pei, F.; Cheng, D.; Zhang, Y.; Cheng, H.; Huang, K.; Yuan, L.; Li, Z.; Xu, H.; Huang, Y. Flame-retardant polyurethane-based solid-state polymer electrolytes enabled by covalent bonding for lithium metal batteries. *Adv. Funct. Mater.* **2024**, *34* (16), No. 2310084.
(25) Wen, S.; Luo, C.; Wang, Q.; Wei, Z.; Zeng, Y.; Jiang, Y.; Zhang, G.; Xu, H.; Wang, J.; Wang, C.; Chang, J.; Deng, Y. Integrated design of ultrathin crosslinked network polymer electrolytes for flexible and stable all-solid-state lithium batteries. *Energy Storage Mater.* **2022**, *47*, 453−461.
(26) Li, Z.; Yu, R.; Weng, S.; Zhang, Q.; Wang, X.; Guo, X. Tailoring polymer electrolyte ionic conductivity for production of low-temperature operating quasi-all-solid-state lithium metal batteries. *Nat. Commun.* **2023**, *14* (1), 482.
(27) Li, Z.; Yu, R.; Weng, S.; Zhang, Q.; Wang, X.; Guo, X. Tailoring polymer electrolyte ionic conductivity for production of low-temperature operating quasi-all-solid-state lithium metal batteries. *Nat. Commun.* **2023**, *14* (1), 482.

https://doi.org/10.1021/acsapm.5c02505
ACS Appl. Polym. Mater. 2025, 7, 12145−12150